Optimizing Measurement Reliability of an IoT Outdoor Air Quality Monitoring System for Tropical Applications Using Simulation and Experimental Approaches

Justin Wee Meng Goh[1], Sien Jie Wong[1], Huiyi Tan[2], Mohamad Nur Hidayat Mat[3], Ruzairi Abdul Rahim[4], Nur Haliza Abdul Wahab[5], Hong Yee Kek[6], Keng Yinn Wong[1*]

[1]Faculty of Mechanical Engineering, Universiti Teknologi Malaysia, 81310 Skudai, Johor, Malaysia
[2]Faculty of Chemical & Energy Engineering, Universiti Teknologi Malaysia, 81310 Skudai, Johor, Malaysia
[3]Faculty of Mechanical and Automotive Engineering Technology, Universiti Malaysia Pahang Al-Sultan Abdullah, 26600 Pekan, Pahang, Malaysia
[4]Faculty of Electrical Engineering, Universiti Teknologi Malaysia, 81310 Skudai, Johor, Malaysia
[5]Faculty of Computing, Universiti Teknologi Malaysia, 81310 Skudai, Johor, Malaysia
[6]School of the Built Environment, University of Reading Malaysia, 79200 Iskandar Puteri, Johor, Malaysia

Corresponding author* email: kengyinnwong@utm.my
Available online 01 March 2026

ABSTRACT

Outdoor air quality monitoring systems (OAQMS) are essential for safeguarding public health and well-being by monitoring environmental changes, especially in urban and industrial areas. This study focuses on the design and development of a protective casing for OAQMS, intended to shield internal electronic components from harsh environmental conditions while maintaining data accuracy and preventing thermal buildup. The system utilizes low-cost sensors to measure PM2.5, PM10, temperature, and relative humidity, integrated with a Raspberry Pi microcontroller. An exhaust fan was incorporated to regulate internal airflow and maintain thermal stability. The casing was developed in accordance with IEC 60529 to ensure resistance against dust and water, enhancing system reliability for outdoor deployment. Validation testing conducted in a controlled environment showed that the casing preserved over 90% of the sensor accuracy.

Keywords: AQMS, Particulate Matter, Casing, Outdoor

1. Introduction

Air pollution is an increasingly critical global issue due to its detrimental impacts on human health, ecosystems, and overall environmental quality. Recent research highlights nitrogen dioxide as a major urban pollutant and a key byproduct of vehicular emissions, significantly affecting air quality in areas surrounding highway infrastructure [1]. In urban and industrial regions, continuous monitoring of air quality is essential to detect harmful pollutants such as particulate matter (PM2.5 and PM10), which are known to cause respiratory and cardiovascular illnesses [2]. OAQMS have been developed to support real-time data collection and provide critical information for environmental analysis and public health decision-making. Poor outdoor air quality poses a substantial and escalating global public health threat, contributing to millions of premature deaths annually, primarily due to chronic exposure to fine particulate matter such as PM2.5 and PM10 [3]. The health implications are extensive, affecting multiple organ systems and all age groups. PM is a major contributor to a wide range of respiratory conditions, including asthma, chronic bronchitis, lung cancer, and respiratory infections [4]. In addition to respiratory issues, air pollution has been strongly linked to cardiovascular diseases such as heart attacks, heart failure, stroke, hypertension, and atrial fibrillation, primarily through mechanisms involving systemic inflammation, oxidative stress, and endothelial dysfunction [3]. Furthermore, mounting evidence points to neurotoxic outcomes, with chronic exposure associated with cognitive decline, Alzheimer's and Parkinson's diseases, schizophrenia spectrum disorders, depression, and anxiety [4]. In men, elevated levels of outdoor air pollution have also been correlated with significant impairments in reproductive health, including reduced semen volume, sperm concentration, motility, morphology, and increased DNA fragmentation index (DFI), which collectively contribute to infertility [5].

Although numerous air quality monitoring technologies are available, many are primarily designed for indoor or controlled environments and are not well-suited for long-term operation in harsh outdoor conditions. For instance, a recent study demonstrated the integration of an IoT-based indoor air quality monitoring system capable of tracking parameters such as PM2.5, PM10, CO_2, O, temperature, and humidity [6]. Similarly, Wong, Tan [7] investigated indoor

air quality by evaluating the filtration efficiency of botanical elements and various filter types. However, outdoor deployment presents additional challenges, as environmental factors like high humidity (above 80%), heavy rainfall, direct sunlight, dust ingress, and fluctuating temperatures (reaching or exceeding 35°C) can compromise sensor accuracy and shorten the lifespan of electronic components [8]. Therefore, there is a critical need for a robust protective casing that can safeguard OAQMS components from environmental stressors while ensuring thermal stability and reliable data acquisition. This study aims to design and develop a cost-effective, weather-resistant casing for outdoor OAQMS applications, particularly for deployment in tropical urban environments such as public parks and roadside monitoring stations. The casing is intended to house low-cost sensors for monitoring PM2.5, PM10, temperature, and relative humidity, and is equipped with a built-in exhaust fan to regulate internal temperature and prevent sensor drift due to heat accumulation. The design adheres to the IEC 60529 standard to ensure protection against dust and water ingress, targeting at least an IP54 rating.

The casing prototype was fabricated using a pre-fabricated junction box made from polyvinyl chloride (PVC) to ensure structural durability under outdoor environment. In addition to providing environmental shielding, the system supports wireless data transmission which provide real time monitoring. To evaluate its performance, computational fluid dynamics (CFD) simulations were conducted to determine the optimal exhaust fan flow rate and analyse internal temperature distribution, followed by experimental validation in a controlled environment. A commercial computational fluid dynamics (CFD) software was to simulate and determine optimal cubic feet per minute (CFM) for the exhaust fan, and to analyse internal temperature distribution.

This study's novelty lies in the integration of CFD-based thermal optimization with practical design validation of a low-cost, weather-resistant OAQMS casing. The proposed design enhances the reliability and operational stability of low-cost sensors under tropical climatic conditions, addressing a key limitation in current OAQMS deployments. Furthermore, the outcomes of this work contribute to the advancement of robust and scalable environmental monitoring solutions that align with the objectives of the United Nations Sustainable Development Goals (SDGs) 11 and 13, particularly in promoting sustainable cities and climate action through continuous outdoor air quality assessment.

2. Overview of OAQMS

An OAQMS integrates various sensors and technologies to assess, monitor, and track air quality levels. These systems are generally divided into two categories: manual and automated. Manual systems primarily rely on laboratory-based methods for analysis. In contrast, automated systems include fixed stations, mobile units, aerial platforms, and satellite-based setups, each designed to measure air pollutants with specific functionalities [9]. These systems play a crucial role in safeguarding human health and the environment by providing accurate and timely information on pollution levels.

Manual monitoring methods are regarded as accurate, but they are limited by their inability to provide real-time information and their reliance on laboratory infrastructure for outdoor air quality monitoring [9, 10]. These factors make manual systems less convenient for contemporary applications, thus prompting a shift towards automated monitoring methods with the capacity for round-the-clock, real-time data collection. The United States Environmental Protection Agency (USEPA) stresses the need for continuous monitoring of major pollutants such as PM, ground-level ozone (O_3), carbon monoxide (CO), sulfur dioxide (SO_2), and nitrogen dioxide (NO_2) as a way of safeguarding public health [11]. Automated OAQMS solutions frequently leverage Internet of Things (IoT) technologies like wireless communication, Wi-Fi, and Bluetooth, which enable real-time forwarding of sensor data to centralized systems for analysis and display [12]. In addition, the systems are regarded as cost-effective due to the utilization of low-cost sensors (LCS), which makes them suitable for large-scale deployment [13]. According to operational attributes and deployment strategies, automated OAQMS can be grouped into various categories such as station-based, satellite-based, mobile-based, and aerial platform-based systems.

Fixed monitoring stations are the most widely implemented due to their simplicity and high measurement accuracy. According to research conducted by E. Collado [14], fixed stations are designed to monitor pollutants such as PM, NO_2, SO_2, PM2.5, PM10, and O_3, and are typically deployed in locations characterized by elevated pollution levels where frequent and consistent monitoring is required [15]. In the referenced study, a fixed station was developed to collect ambient temperature, humidity, and air pollutant data, in addition to meteorological variables such as wind speed, wind direction, and precipitation. The system utilizes two microcontrollers to manage multiple sensors, thereby enhancing data accuracy and system functionality. Data transmission is facilitated through an Ethernet connection, ensuring stable and high-speed communication with the internet, where data is displayed via a user-friendly interface. The system's performance was validated by comparison with a commercial-grade air monitoring device, the Aeroqual Series 500. The results demonstrated minimal error, thereby confirming the reliability of the fixed station for environmental monitoring purposes. By integrating comprehensive engineering principles, validated simulation methods, and intelligent environmental sensing technologies, the developed OAQMS offers a scalable and sustainable solution for addressing air quality monitoring challenges in urban and industrial environments.

3. Methodology

3.1 Development of an IoT-Based OAQMS

This study primarily concentrates on the design and implementation of an IoT integrated smart sensor system for real-time air quality monitoring. The systematic development process of the proposed OAQMS is depicted in Figure 1.

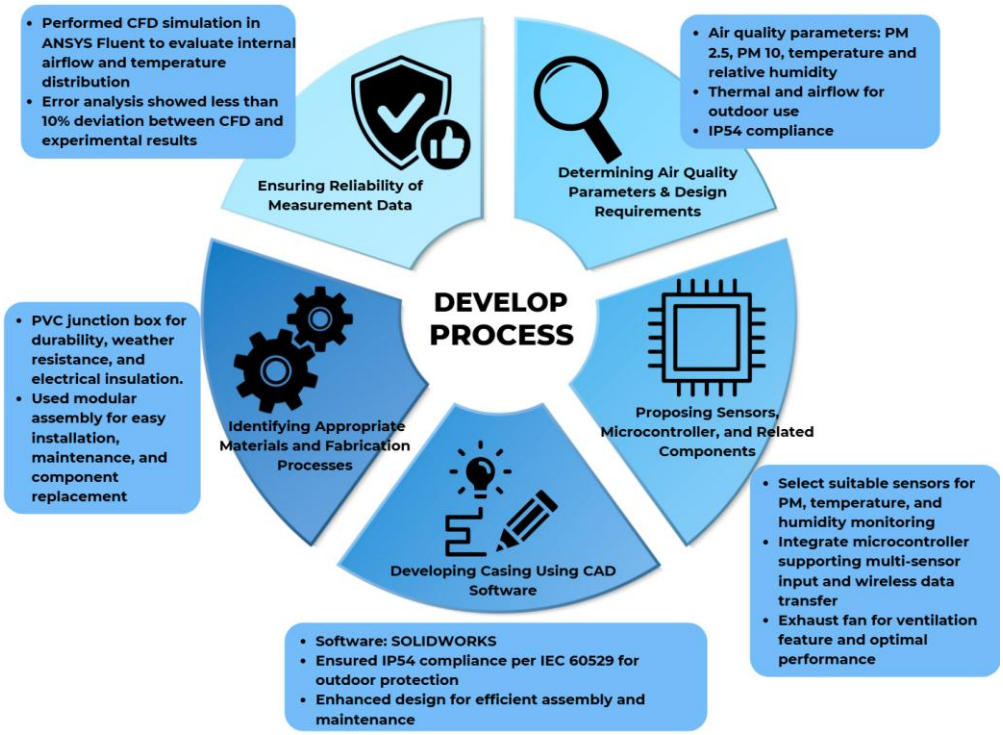

Figure 1. Process of developing a casing for OAQMS for tropical applications

The development of the outdoor air quality monitoring system was systematically structured into several key stages to ensure optimal functionality and environmental suitability. Initially, relevant air quality parameters were identified, followed by the establishment of corresponding design specifications tailored for outdoor applications. Appropriate sensors, a microcontroller, and supporting electronic components were then selected based on performance, durability, and compatibility criteria. Subsequently, the system casing was designed using CAD software to optimize airflow and component arrangement. Material selection was conducted with consideration for weather resistance and structural integrity, culminating in the fabrication of the casing. Finally, comprehensive performance validation was carried out to evaluate the operational accuracy, data reliability, and overall system robustness under real-world outdoor conditions.

3.2 Determination of Relevant Air Quality Monitoring Parameters and Design Specification

The design and development of the OAQMS enclosure emphasized the creation of durable and weather-resistant housing capable of safeguarding internal components from environmental conditions while maintaining the accuracy of sensor measurements. The development process commenced with the identification of key air quality parameters: PM2.5, PM10, temperature, and relative humidity, essential for assessing atmospheric pollution, particularly in urban and industrial settings [16]. To fulfill the functional and protective requirements, the enclosure was designed in accordance with the International Electrotechnical Commission (IEC) 60529 standard, which defines the levels of protection provided by enclosures for electrical equipment. Compliance with this standard enabled the OAQMS to attain a suitable Ingress Protection (IP) rating, thereby enhancing its durability and operational reliability [17].

The casing was conceptualized and structurally modeled using commercial computer-aided design (CAD) software, facilitating the incorporation of critical structural and operational features. These included precisely allocated compartments for sensor and electronic module installation, optimized air circulation channels, and strategically placed access openings to facilitate wiring, system calibration, and maintenance. The final assembly comprised two main components: a protective base housing and a removable top cover that enabled straightforward access to the internal electronics. The protective casing had dimensions of 142 mm (W) × 226 mm (L) × 304 mm (H), and the roof with dimensions of 202 mm (W) × 295 mm (L) × 25 mm (H).

To ensure thermal regulation within the enclosure and to support accurate sensor performance, multiple air intake vents were incorporated at the lower section of the casing. These were complemented by an exhaust outlet at the upper section, integrated with a direct current (DC) cooling fan. This ventilation arrangement facilitated continuous internal airflow and mitigated heat buildup from electronic components [14]. The internal layout of the system was carefully planned to optimize sensor placement. Particulate matter sensors were installed near the air inlets to ensure immediate interaction with ambient air, thereby enhancing responsiveness and measurement accuracy. Conversely, temperature and humidity sensors were positioned away from heat-emitting components such as the Raspberry Pi, minimizing thermal interference and preserving the integrity of recorded data. This comprehensive design strategy ensured both the mechanical protection of internal hardware and the functional precision of the monitoring system. As a result, the OAQMS is capable of delivering consistent and reliable performance under a variety of environmental conditions, making it a suitable solution for extended outdoor air quality monitoring applications across diverse geographical and climatic settings.

3.3 Selection of Sensors, Microcontroller and Electronic Components

The selection and strategic arrangement of electronic components played a critical role in ensuring the accuracy and reliability of the developed of the developed OAQMS. The selected sensors demonstrated the capability to accurately detect the targeted pollutants while withstanding extreme environmental conditions, such as the elevated temperatures and high humidity levels characteristic of tropical rainforest climates. To maintain consistent system performance under these conditions, the integration of reliable power supply units and high-performance microcontrollers was essential. Additionally, a DC exhaust fan was implemented to facilitate internal air circulation, thereby reducing thermal buildup and ensuring that sensors operated within their designated temperature thresholds [14]. The deliberate selection of components specifically suited for harsh environmental exposures enabled the OAQMS to deliver stable long-term data acquisition and maintain operational integrity. Table 1 summarizes the primary electronic components employed in this study, while Figure 2 illustrates the schematic configuration of the IoT-based smart sensor network, including the Raspberry Pi, peripheral components, and the corresponding database interface.

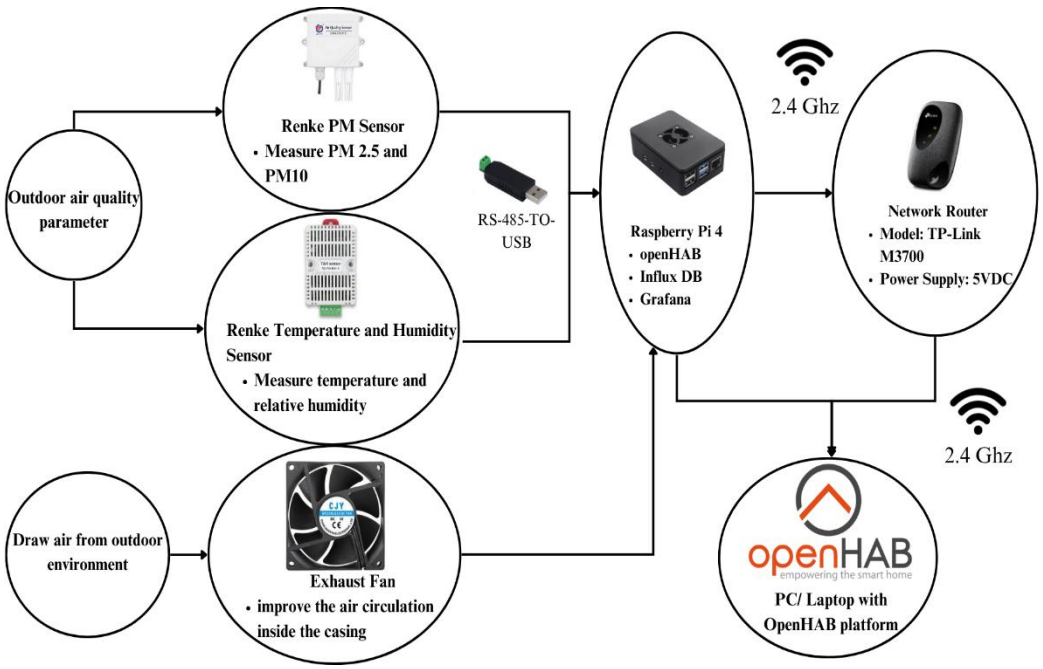

Figure 2. The schematic diagram of the IoT smart sensors, raspberry pi, related components and database linkage

Table 1. Specifications of the main electronic components in the OAQMS

No	Components	Brand	Model	Parameter	Response time	Output signal	References
1	Renke pm2.5 air quality sensor	Renke	RS-PM-*−2	PM2.5 and PM10	≤90s	RS485/0-5V/0-10V/4-20mA	[18]
2	RS-WS-N01-8-EX	Renke	RS-WS-N01-8	Temperature	≤25s	RS485	[19]
			RS-WS-N01-8	Humidity	≤8s	RS485	
3	Microcontroller	Raspberry pi	4 Model B	-	Instant	-	[20]
4	DC 5V exhaust fan	-	8025-12-HX2.54 2pin	Exhaust fan	Instant	12V (XH2.54 2pin)/ (0.2-0.3) A +/-10%	[21]

3.4 Prototype Fabrication and Setup

The fabrication and assembly of the OAQMS casing was carried out with an emphasis on durability and weather resistance, ensuring the system's suitability for prolonged outdoor deployment. The main body of the protective casing was constructed using a pre-fabricated PVC junction box, selected for its high resistance to water ingress, corrosion, and dust accumulation[11]. To enhance protection from environmental factors such as direct sunlight and rainfall, the top cover was fabricated using aluminum alloy 1100, known for its excellent thermal and corrosion resistance properties [11, 22]. The material properties of the aluminum alloy are summarized in Table 2.

Table 2. Material properties of aluminum alloy 1100

Aluminium alloy	Density	Melting Range	Thermal Conductivity	Specific Heat Capacity	Electrical Resistivity
1100	2.71 g/cm³	643–657 °C	~222 W/m·K	~900 J/kg·K	~2.99×10⁻⁸ Ω·m

To facilitate optimal air exchange within the enclosure, air inlet vents were strategically positioned at the lower section of the casing to allow ambient air intake. A direct current (DC) exhaust fan was installed at the upper section to promote continuous airflow, thereby reducing internal heat buildup and maintaining a stable thermal environment. The internal configuration was deliberately organized to enhance measurement accuracy, with particulate matter sensors placed adjacent to the air inlets to allow direct exposure to ambient air. Conversely, temperature and humidity sensors were situated away from heat-emitting components to minimize thermal distortion.

The roof was supported using C-shaped brackets formed from combined stainless-steel L-brackets with dimensions of 16 mm (W) × 50 mm (L) × 50 mm (H) which provide strong mechanical stability. All electronic components, including the Raspberry Pi 4, environmental sensors, and cooling fan, were securely mounted within the enclosure. Cable routing was carefully managed to prevent the obstruction of airflow and to maintain an organized internal layout.

Following assembly, the complete OAQMS unit underwent preliminary functional testing and outdoor trials to evaluate the system's structural robustness, ventilation performance, and overall operational reliability prior to the formal validation phase. Figure 3 presents the fabricated OAQMS prototype, while Figure 4 provides a detailed view of the internal sensor and electronic component placement.

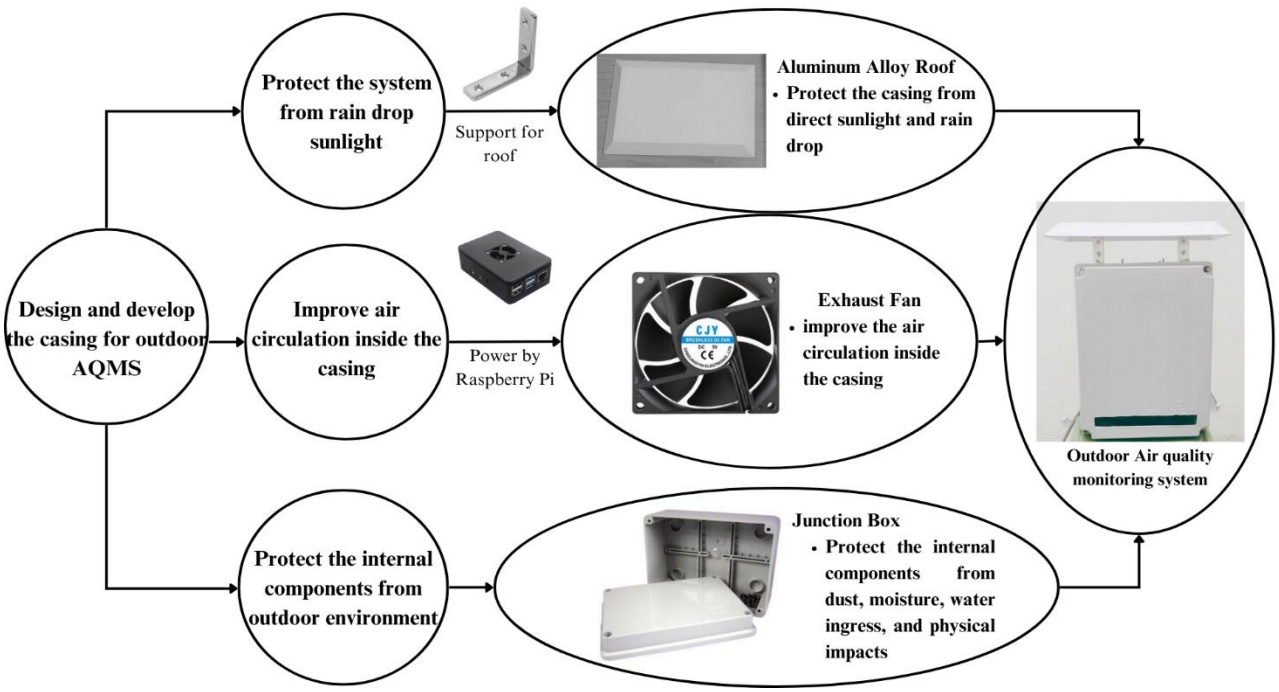

Figure 3. Development prototype of OAQMS

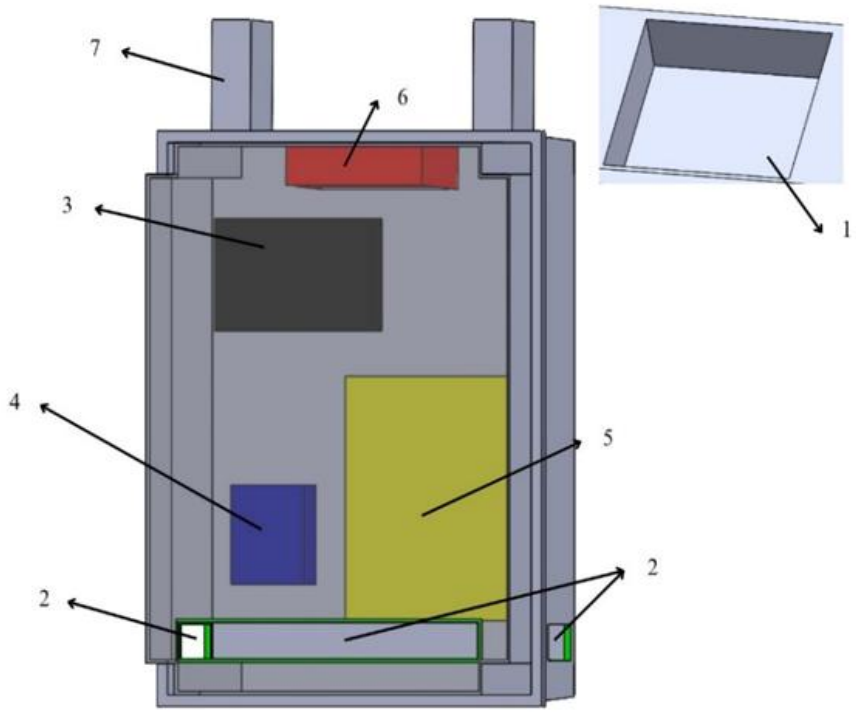

Figure 4. Isometric view of the protective casing (1, exhaust outlet vent; 2, air inlet vent; 3, Raspberry Pi 4, temperature and humidity sensor; 5, PM sensor; 6, DC exhaust fan; 7, support for the roof)

3.5 Validation Testing

To evaluate whether the integration of the protective enclosure influenced the performance and accuracy of the OAQMS, a structured validation procedure was carried out. This validation was designed to assess the system's performance under two distinct configurations: one with the sensors and electronic components fully exposed, without the casing and the other with all components enclosed within the custom-fabricated protective casing.

The validation experiments were conducted in a controlled indoor environment with stabilized ambient conditions, particularly temperature and airflow velocity. An anemometer was utilized to measure both parameters temperature and airflow at the air outlet of the room's air conditioning unit, as depicted in Figure 5. Based on the initial readings, adjustments were made to the air conditioning settings to establish and maintain a stable testing environment prior to data acquisition. During the validation process, the ambient temperature was consistently maintained at 18.1 °C, with an airflow velocity of 0.3 m/s. These controlled conditions were deliberately selected to minimize environmental variability, thereby enhancing the reliability and consistency of the performance evaluation. The experimental setup for the validation is presented in Figure 5.

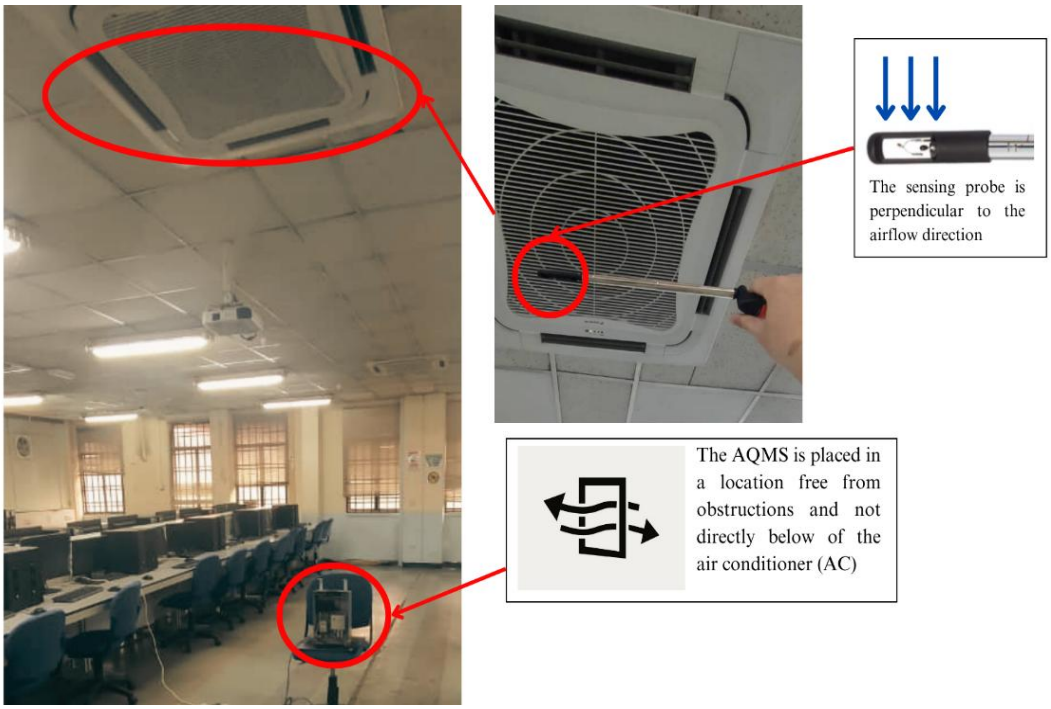

Figure 5. The setup for the validation test.

To ensure the reliability and accuracy of the experimental results, several precautionary measures were implemented prior to the commencement of the validation tests. These measures were specifically designed to mitigate potential interferences from external factors such as ambient temperature variations, heat accumulation within the enclosure, airflow inconsistencies, and thermal output from the Raspberry Pi.

To ensure that the data collected accurately reflected the operational performance of the OAQMS, the following systematic procedures were carried out:

1. The validation was conducted in a closed control room to eliminate the influence of human activity and prevent the intrusion of outdoor air, both of which could affect the ambient temperature and airflow.
2. Prior to each test, the OAQMS was allowed to reach thermal equilibrium with the room environment to prevent residual heat from skewing the sensor measurements.
3. After each trial, the Raspberry Pi and internal components were given sufficient time to cool before initiating the subsequent test.
4. A thermal infrared thermometer (thermal gun) was used to verify that no residual heat was present within the enclosure prior to data collection.
5. The OAQMS was positioned in an unobstructed, clean area to ensure uniform airflow and prevent localized disturbances.

The configuration in which the OAQMS operated without the protective casing was designated as the reference case, representing an optimal condition where the sensors were fully exposed to ambient air without physical barriers [16]. This served as the performance benchmark against which the enclosed configuration was evaluated. Figure 6 presents the experimental setups used for both the uncased and cased validation configurations.

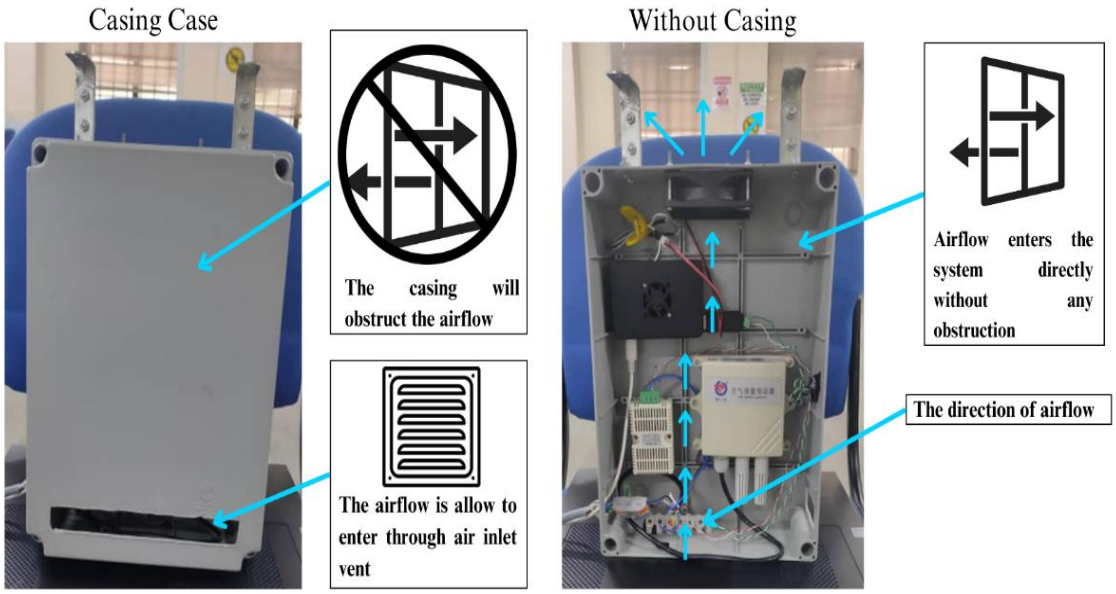

Figure 6. OAQMS setup for validation process (a) casing case (b) without casing case

Throughout the validation process, temperature and relative humidity data were continuously monitored and transmitted to Grafana, an online visualization and analytics platform. This enabled real-time observation of system performance. Upon completion of the monitoring phase, the recorded data were exported in Comma-Separated Values (CSV) format for comprehensive post-processing and analysis. To evaluate potential discrepancies between the two system configurations (with and without casing), the percentage error for each parameter was calculated using Equation 1 [23]. This analytical approach was essential in assessing whether the thermal and airflow dynamics introduced by the protective casing had a measurable impact on sensor outputs. The resulting error analysis served to validate the integrity, accuracy, and operational reliability of the enclosure design, confirming its suitability for consistent outdoor deployment.

$$Percentage\ error = \frac{(|Result_{with\ casing} - Result_{without\ casing}|)}{Result_{without\ casing}} \times 100\% \quad (1)$$

3.6 Evaluation of the Optimal Cubic Feet per Minute (CFM) of the Exhaust Fan for OAQMS

To evaluate and optimize the thermal performance of the developed casing, a Computational Fluid Dynamics (CFD) simulations were conducted using ANSYS Fluent 2021 R2. The aim was to determine the optimal cubic feet minute (CFM) of the exhaust fan required to maintain internal temperatures below the critical threshold of 54 °C under outdoor environmental conditions. Figure 7 illustrated a systematics procedure to evaluate the optimal CFM of the exhaust fan.

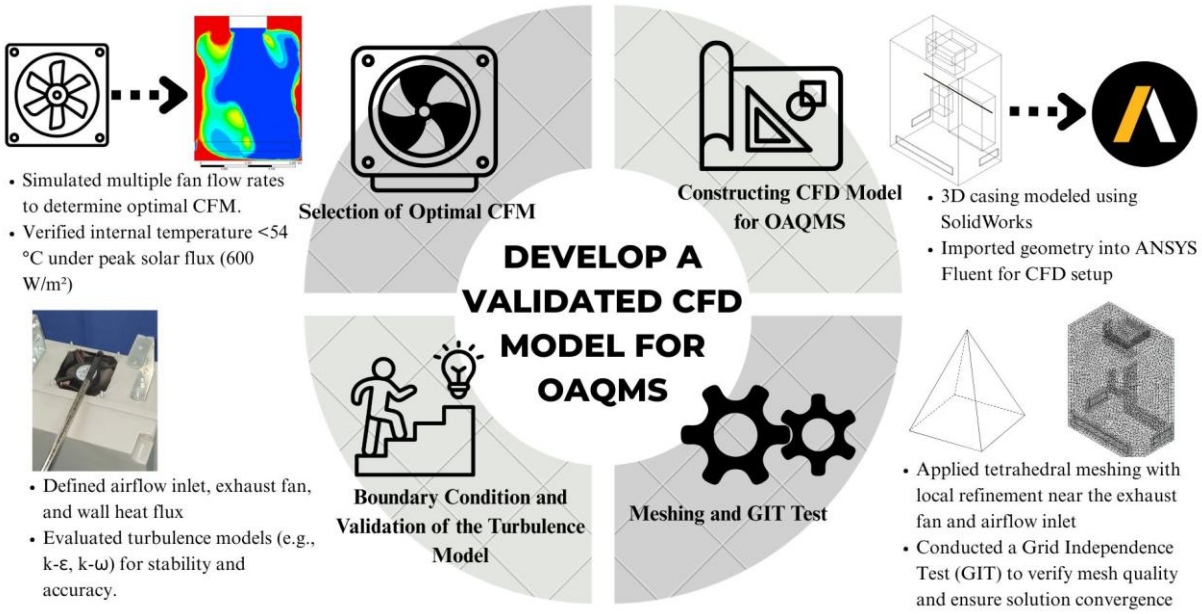

Figure 7. Process of develop a validated CFD model for OAQMS for tropical application

3.7 Constructing CFD Model for OAQMS

The CAD model of the OAQMS casing was constructed using SolidWorks and imported into ANSYS Fluent for simulation. The model included all relevant internal components such as the Raspberry Pi, PM sensor, temperature and humidity sensor, and the DC exhaust fan. Precise physical dimensions from the fabricated prototype were applied to ensure simulation fidelity.

The outdoor OAQMS casing was simplified from a junction box into a basic cuboid structure. The casing region has dimensions of 226 mm (L) × 142 mm (W) × 304 mm (H). Two sensors were included in the model a PM sensor with dimensions of 110 mm (L) × 44 mm (W) × 135 mm (H), and a temperature and humidity sensor with dimensions of 45 mm (L) × 28 mm (W) × 55 mm (H). Additionally, a Raspberry Pi was modelled with dimensions of 95 mm (L) × 32 mm (W) × 62 mm (H). The geometric features of the model were simplified, as the detailed structures were unlikely to significantly affect the overall simulation results.

Air was supplied to the casing using an exhaust fan placed at the centre of the top plane of the casing, with dimensions of 80 mm (L) × 80 mm (W) × 2.5 mm (H). Air was drawn into the system through three rectangular inlet vents: one measuring 186 mm (L) × 2 mm (W) × 20 mm (H), and two measuring 60 mm (L) × 2 mm (W) × 20 mm (H). Figure 8 provides the isometric view of the CFD model.

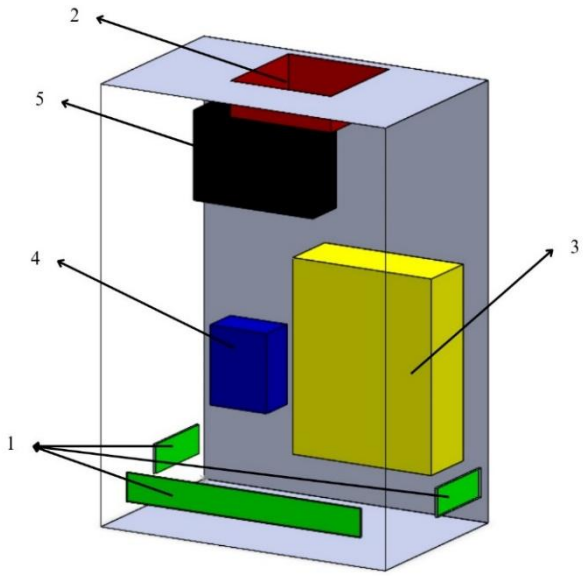

Figure 8. Isometric view of CFD model (1, air inlet vent; 2, exhaust fan; 3, PM sensor; 4 temperature and humidity sensor; 5, Raspberry Pi 4)

3.8 Meshing and Grid Independent Test (GIT) of the OAQMS

The casing was discretized using unstructured tetrahedral mesh elements. Unstructured tetrahedral mesh elements are effective for capturing complex surface profiles [24]. Tetrahedral meshes are commonly utilized in engineering due to their well-established generation techniques and optimization strategies. However, tetrahedral meshes are limited by factors such as element size, mesh density, and element quality [25]. Mesh refinement was applied around critical regions including air inlet vents and the exhaust outlet to accurately capture flow behaviour and temperature gradients as shown in Figure 9. The enhanced wall treatment function was enabled to accurately capture the detailed characteristics of boundary layer flow [26]. The convergence criterion was set at 1×10^{-4} for equations of continuity, x-velocity, y-velocity, z-velocity, turbulent kinetic energy, and turbulent dissipation, whereas the energy equation was fixed at 1×10^{-9}, based on the past study recommendation [27].

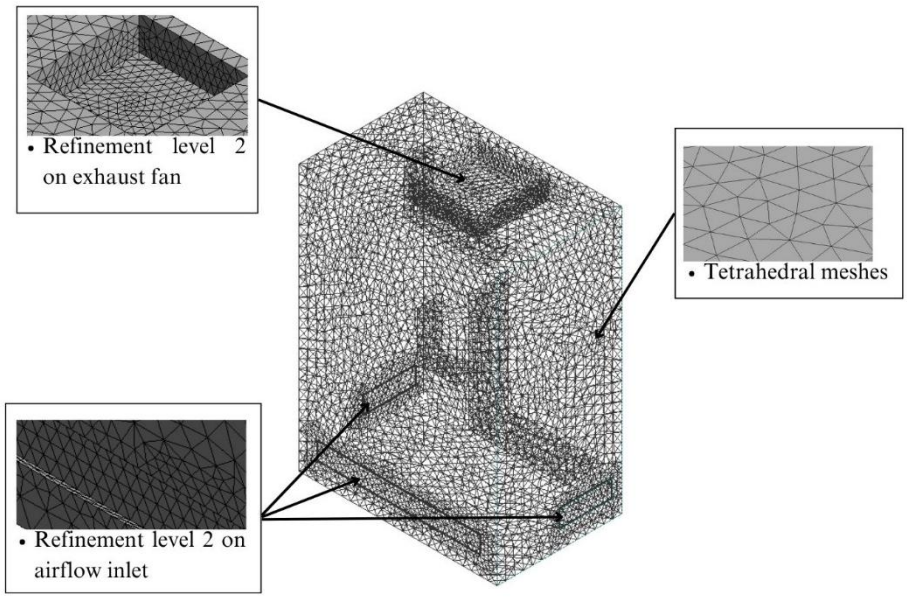

Figure 9. Meshing of the OAQMS isometric view

Grid Independence Test (GIT) was performed to ensure that mesh refinement had minimal impact on the simulation results, thereby validating the accuracy and reliability of the selected mesh configuration. The primary objective of this test was to determine the minimum mesh resolution beyond which further refinement would not produce significant changes in the predicted airflow behaviour. This approach minimizes discretization errors while maintaining a practical balance with computational cost.

GIT was conducted using 3 different mesh configurations. The model was initially meshed at 80k elements, followed by 200k and 300k elements. The influence of mesh size was compared through the simulated airflow velocity result along the geometry centre line from coordinates (0, 0.152, 0.03) to (0.226, 0.152, 0.03) as shown in Figure 10. A total of 100 evenly spaced data points were extracted along this centreline to ensure consistent sampling.

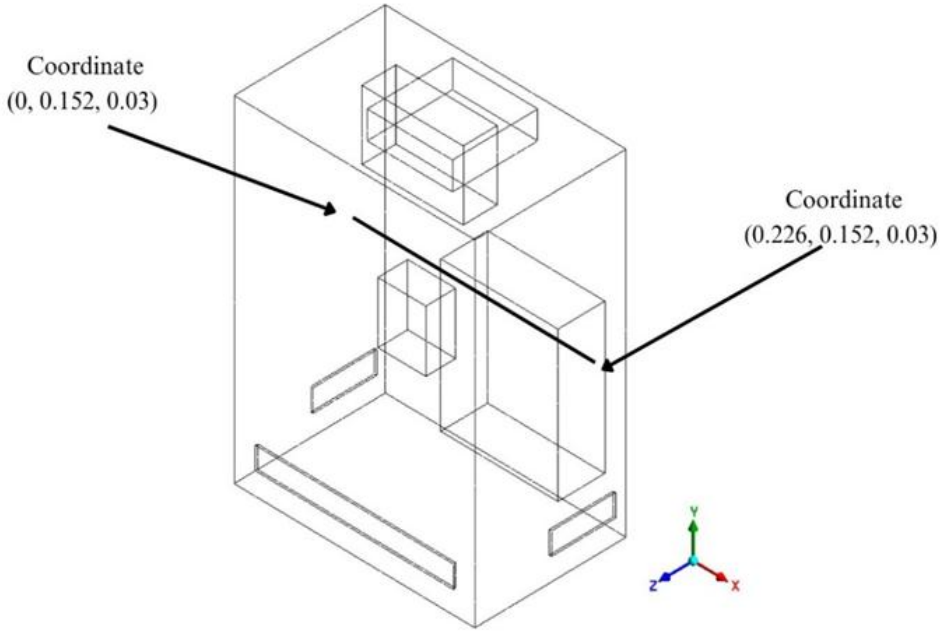

Figure 10. Geometric centre line that cuts through the middle of the OAQMS

Figure 11 shows that grid independence was achieved with mesh sizes of 200k and 300k of unstructured tetrahedral elements, as indicated by the negligible variation of airflow velocity results. Further increases in element count beyond this range resulted in minimal changes, with the simulation outputs plateauing at the peak of the graph. The velocity profiles exhibited similar trends and began to converge at 200k elements. Nonetheless, this study adopted a mesh size of 300k elements to ensure higher reliability and accuracy in the simulation outcomes.

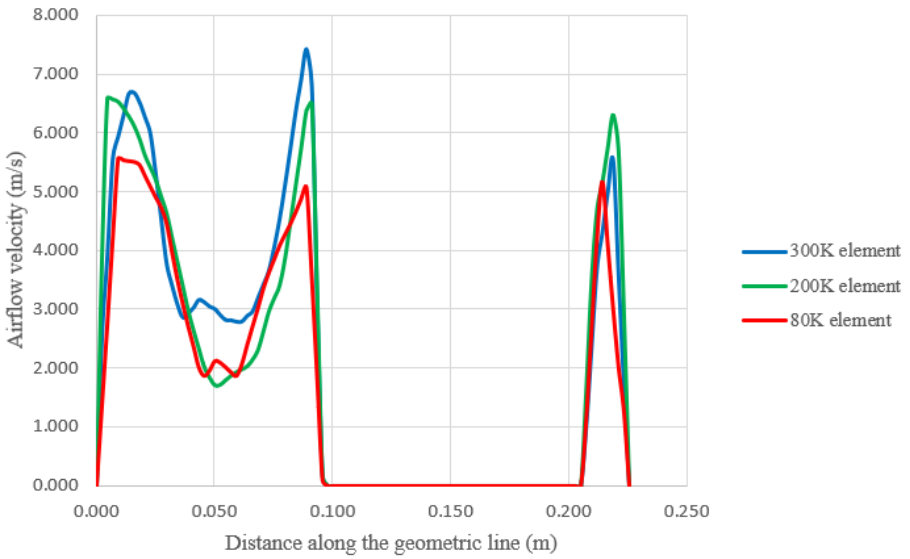

Figure 11. Variation of airflow velocities along the geometric line across OAQMS CFD model considering different mesh densities

3.9 Meshing and Grid Independent Test (GIT) of the OAQMS

Several assumptions were made prior to setting up the boundary conditions in order to simplify the CFD model and reduce computational complexity while maintaining simulation accuracy, as shown in Table 3.

Table 3. Assumptions for boundary condition

No.	Assumption	Remarks/ Justification
1	Steady-state thermal performance [28]	To evaluate internal temperature under stable conditions with maximum heat flux (measured) and ignoring outdoor effects to focus on fan cooling performance.
2	The casing was assumed to be well-insulated	This reduces heat loss to the environment and allows the simulation to focus on internal temperature behaviors, simplifying thermal boundary conditions.
3	Heat from radiation was considered to be uniformly distributed across the casing surface	Assuming uniform distribution simplifies modelling while still representing a worst-case heating scenario.
4	Uniform heat flux distribution	This assumption ensures consistent thermal input across the casing surface, reducing mesh sensitivity and simulation time, while still capturing overall thermal effects.
6	The internal airflow was assumed to be incompressible	Airflow velocity is low, compressibility effects around the fan are minimal and negligible for thermal simulation
7	Gravitational acceleration was set to 9.81 m/s²	Standard value used to account for natural convection effects, accurately represents Earth's gravity at sea level
8	Heat generated by the Raspberry-pi and sensors was considered negligible	The heat contribution from these components are minimal compared to solar heat flux, and excluding it helps simplify the model.
9	The influence of natural wind inside the casing was considered negligible	The airflow inside the casing is driven by the exhaust fan, while outdoor air has negligible impact due to casing

The CFD model was set up to simulate the effect of solar heat exposure on the casing while assessing the efficiency of the exhaust fan in dissipating accumulated heat. The external heat load was modelled as a constant surface heat flux of 600 W/m² applied to the top surfaces of the casing, simulating intense solar radiation typical in tropical outdoor environments. The heat flux was determined through thermal measurements obtained using an infrared thermal scanner during peak daytime exposure as shown in Figure 12 and subsequently verified using Fourier's law of heat conduction to estimate the equivalent heat flux based on the measured surface temperature gradients.

Figure 12. (a) Temperature outside the casing (b) temperature inside the casing

Internal heat generation from electronic components was assumed negligible for short-term operation, based on thermal characterization of the Raspberry Pi and sensor modules. The exhaust fan airflow performance was characterized using a P–Q curve, constructed from empirical data obtained with an anemometer to ensure accurate representation of the fan operating behavior within the CFD model as shown in Figure 13. Boundary conditions were defined as shown in Table 4.

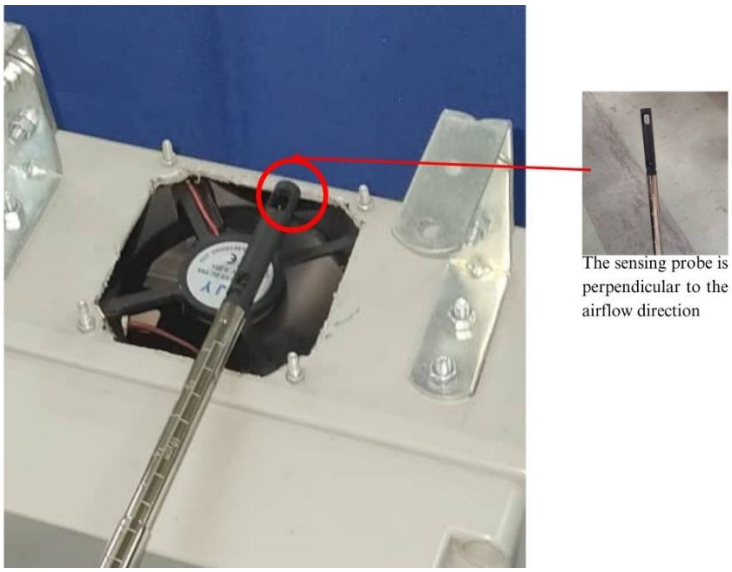

Figure 13. The measuring of the exhaust fan airflow using anemometer

Table 4. Boundary conditions prescribed on the CFD model of OAQMS

Item	Boundary condition	Value
Air inlet vent	Velocity inlet	-
Exhaust fan	Exhaust fan	Based on P-Q curve of the exhaust fan (User-defined function) as shown in Figure 14
Sensors and Raspberry-Pi	Isothermal wall	Heat release by the sensors and Raspberry-Pi are neglected
Casing wall	Wall (heat flux)	600 W/m^2 (measure by using thermal scanner)

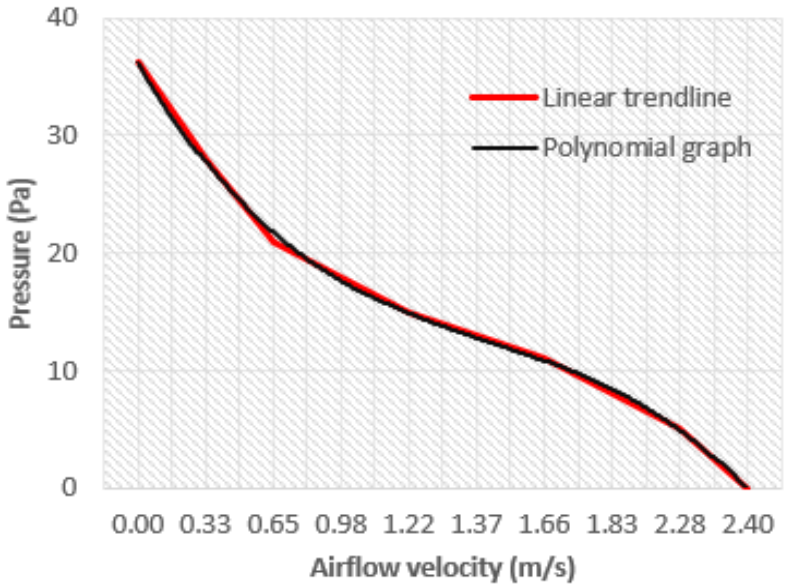

Figure 14. P-Q curve for the exhaust fan to reflects the actual fan suction condition

In the validation phase, a total of 3 turbulent models based on Reynolds-Averaged Navier Stokes (RANS) model were tested. The models were Shear-Stress Transport (SST) k-ω, Re-Normalisation Group (RNG) k-ε and standard k-ε. These turbulent models have been widely adopted in past enclosed environmental airflow study, which proven reliable for low turbulent condition [29]. Hence, these models were employed to simulate the internal airflow velocity of the OAQMS and the results were compared with the measured data from experimental study [30]. The experimental result obtained through measurement using an anemometer to measure the internal airflow velocity of the OAQMS. Due to the small size of the casing, it was not possible to place the anemometer inside the casing. Thus, the airflow velocity was measured only at the base of the casing, as shown in Figure 15. The results of simulation and experimental data are shown in Figure 16. Among the three turbulent model, the SST k-ω model has the lowest relative error, and hence was selected as the validated model for subsequent simulation.

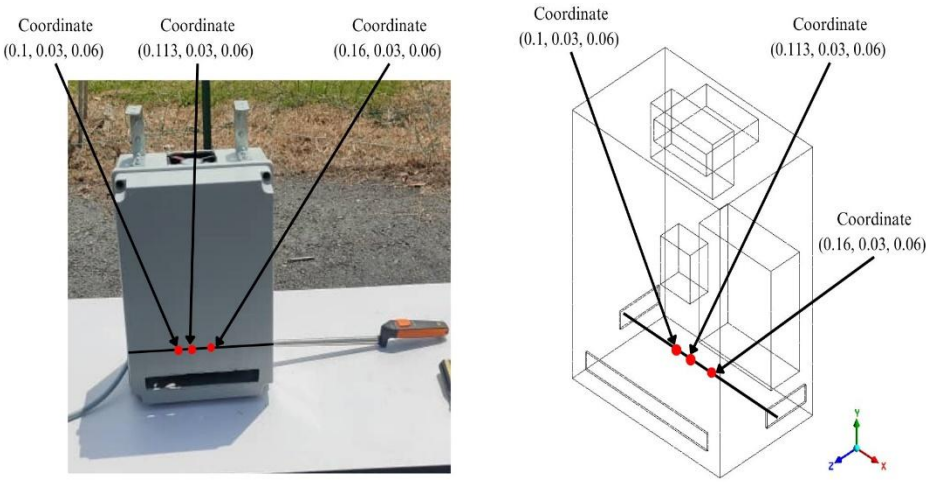

Figure 15. Measurement coordinate of the airflow velocity

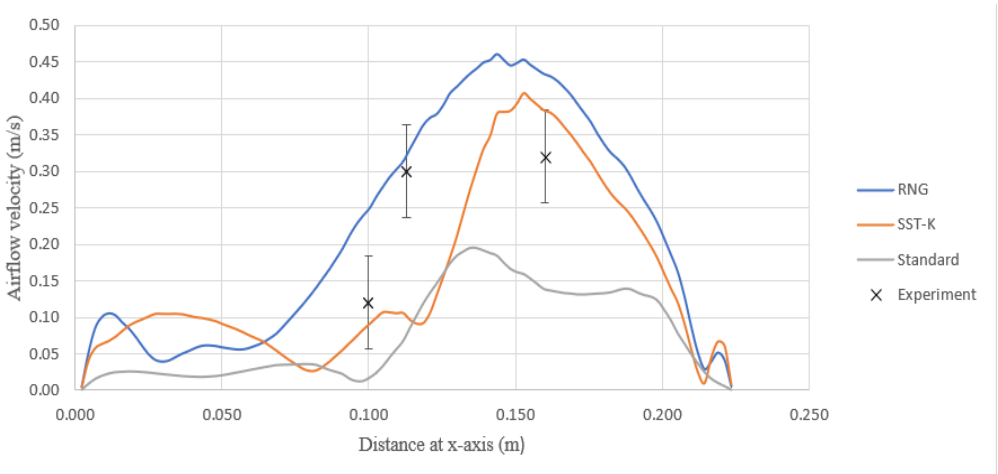

Figure 16. Validation of turbulence model

3.10 Optimal CFM of Exhaust Fan Determination

The determination of the optimal Cubic Feet per Minute (CFM) for the exhaust fan was critical to maintaining the internal temperature of the OAQMS casing below the threshold of 54 °C, which ensures the safe and reliable operation of sensitive electronic components. This was achieved through a comparative CFD simulation study, which evaluated airflow and temperature distribution for multiple fan configurations.

The CFM was varied both increased and reduced based on the airflow velocity and pressure characteristics of the exhaust fan. CFM was calculated using Equation 2 based on the exhaust fan maximum airflow velocity. Table 5 presents the CFM values corresponding to three different maximum airflow velocities of the exhaust fan for each case study. To ensure uniformity in simulation, the number of meshing elements as well as turbulence model was kept as presented in reference case.

Table 5. The relative error for each turbulence model

Case	CFM (m^3/min)	Airflow velocity
Baseline Case	25.4 CFM (0.72 m^3/min)	2.40 m/s
Case 1	44.18 CFM (1.25 m^3/min)	4.15 m/s
Case 2	23 CFM (0.65 m^3/min)	2.16 m/s

All boundary conditions were also kept consistent, with the only change in the exhaust fan pressure and velocity. The performance evaluation in all the configurations under consideration was made with respect to the reference case for determining the impact of various CFM in enhancing internal airflow as well as the heat performance of OAQMS.

$$CFM = \frac{(V \times A)}{0.028} \quad (2)$$

Where V is air velocity (m/min), A is cross section of the exhaust fan, and r is radius of fan (40mm).

4. Results and Discussion

4.1 Validation of the Operational Accuracy of the OAQMS

To assess the measurement accuracy of the developed OAQMS, a validation experiment was performed by comparing sensor outputs under two distinct configurations: (i) an open configuration, wherein the sensors were fully exposed to the surrounding environment, and (ii) an enclosed configuration, with sensors housed within the fabricated protective casing. The primary objective of this validation was to examine whether the presence of the casing introduced any measurable impact on temperature and relative humidity readings. Due to potential disturbances in the controlled room environment such as door openings and human activity the standard data collection interval of 30 minutes was reduced to 6 minutes. This adjustment was made to minimize the influence of short-term environmental fluctuations and to improve the reliability of the comparative analysis.

Sensor data from both configurations were monitored in real time via Grafana, an online platform for continuous visualization and performance tracking. Following each 6-minute sampling interval, data were exported in Comma-Separated Values (CSV) format and analysed using Microsoft Excel. The percentage error between the two configurations was then calculated to evaluate measurement deviation. Table 6 summarizes the recorded temperature and relative humidity values for both setups, including the corresponding percentage errors.

Table 6. Comparison of temperature and relative humidity measurements with and without protective casing for validation purposes

	Temperature (°C)			Relative humidity (%)		
	Without Casing	Casing Case	Percentage error	Without Casing	Casing Case	Percentage error
	21.68	21.80	0.57	64.46	63.77	1.07
	21.60	21.80	0.95	64.71	64.63	0.11
	21.59	21.73	0.66	64.25	62.93	2.05
	21.55	21.62	0.31	63.87	61.82	3.22
	21.49	21.45	0.18	63.41	60.87	4.01
	21.45	21.30	0.69	62.80	60.57	3.55
Average Percentage error (%)			0.56			2.34

The results show that the average percentage error for temperature was only 0.56%, while that for relative humidity was 2.34%. These values suggest that the protective casing has a minimal impact on sensor accuracy, particularly for temperature measurements. Slightly higher deviations observed in humidity readings are likely due to minor variations in airflow patterns within the enclosure.

4.2 Validation of the Internal Accuracy of the OAQMS

The simulation results focused on identifying hotspot areas and evaluating airflow circulation within the OAQMS casing by analyzing temperature and airflow velocity contours at cross-sectional planes (Z = 20 mm and Z = 50 mm), which helped detect heat concentration near critical components such as the Raspberry Pi and PM sensor, as well as assess whether air movement was sufficient to prevent heat buildup.

Based on the simulation result shown that, Case 1 (44.18 CFM) demonstrated the most effective thermal regulation within the OAQMS casing. The Reference Case exhibited significant heat buildup around critical components such as the Raspberry Pi and PM sensor, primarily due to airflow stagnation, which limited heat dissipation. While this setup may suffice under mild outdoor conditions, it may not perform reliably in hot or high-radiation environments.

Case 2, using a lower CFM fan, showed limited cooling improvement, with persistent hotspots and inadequate airflow circulation near the top section of the casing. In contrast, Case 1 higher airflow capacity promoted active and consistent internal circulation, reducing edge temperatures and eliminating stagnant zones. This resulted in a more balanced thermal profile and minimized the risk of localized overheating. An exhaust fan rated at 44.18 CFM is therefore recommended to ensure the OAQMS maintains stable operation and protects electronic components under harsh environmental conditions.

To validate this recommendation, Table 7 presents a comparative summary of temperature and airflow velocity contours across all cases. Table 7 clearly highlights the influence of exhaust fan capacity on internal cooling performance, emphasizing the importance of selecting a fan with sufficient airflow to ensure system reliability.

Table 7. Simulation result for Baseline case. case 1 and case 2

Case	Baseline Case	Case 1	Case 2
Temperature contour on Plane Z = 50 mm	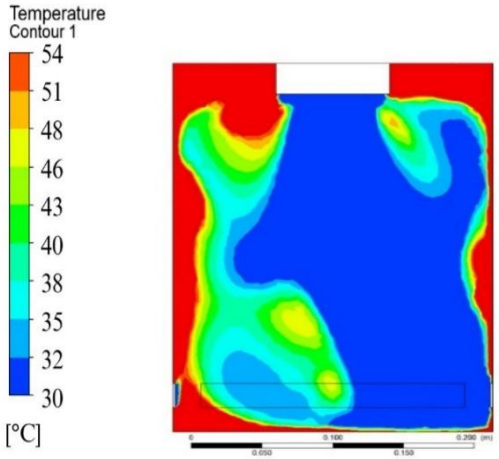	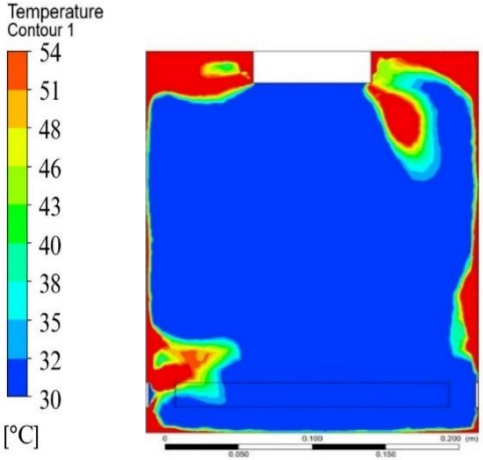	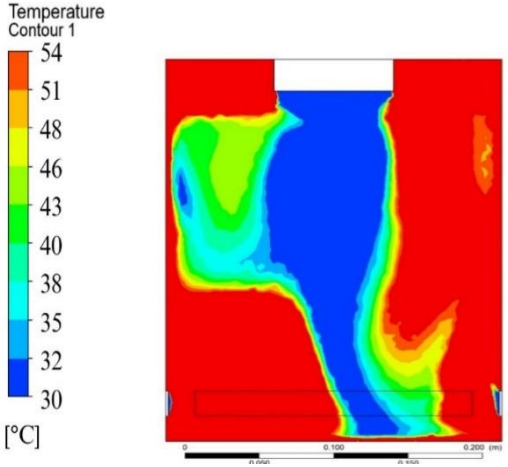
	Hotspots of approximately 54 °C were observed along the edges and at the lower-left corner of the casing	Improvement in CFM gradually reduced the high temperature regions inside the casing, lowering the temperature to 30 °C Compare to References Case, Case 1 demonstrated that approximately 80% of the high-temperature regions were eliminated with high CFM of the exhaust fan	Reduction in CFM led to a gradual increase of the high temperature regions approximately 54 °C within the casing, especially on the right-hand side Compare to References Case, Case 2 exhibited approximately 70% of the casing shows high-temperature with low CFM of the exhaust fan

Airflow velocity contour on plane Z = 50 mm	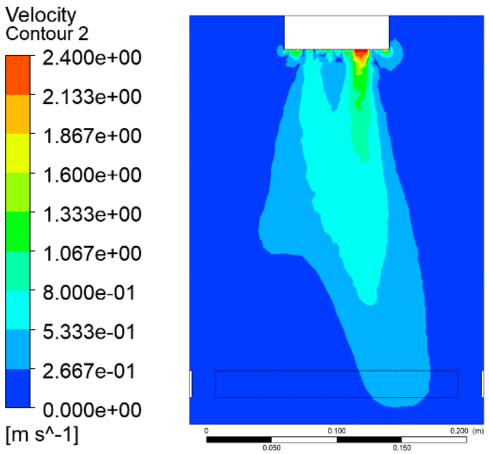	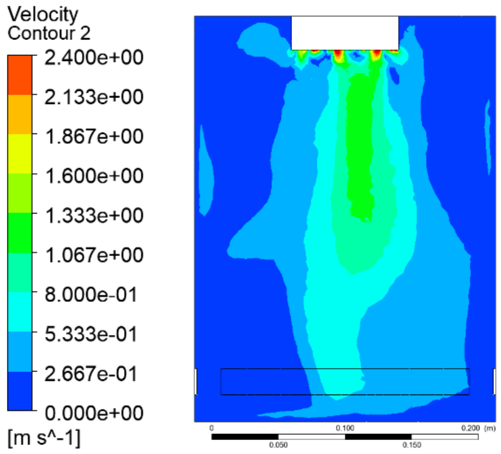	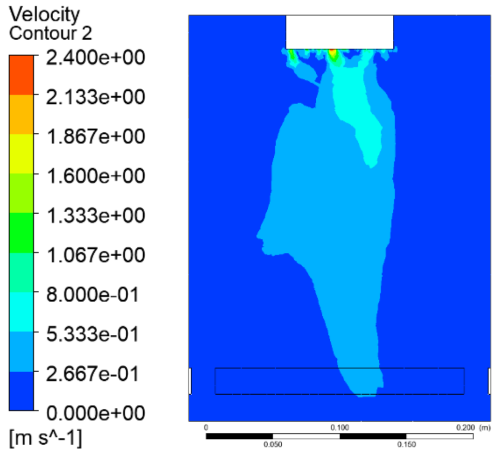
	The maximum airflow velocity at the central region ranged from 0.27 m/s to 0.8 m/s	Improvement in CFM led to an increase in airflow velocity, ranged from 0.27 m/s to 1.6 m/s at the central region, accompanied by an expansion of the airflow circulation area The enhancement in CFM, the maximum airflow velocity was improved from 0.8 m/s to 1.6 m/s	Reduction in CFM led to a decrease in airflow velocity, ranged from 0.27 m/s to 0.53 m/s in the central region, with a corresponding reduction in the airflow circulation area The reduction in CFM resulted decrease in maximum airflow velocity from 0.8 m/s to 0.53 m/s.

Temperature contour on plane Z = 20 mm	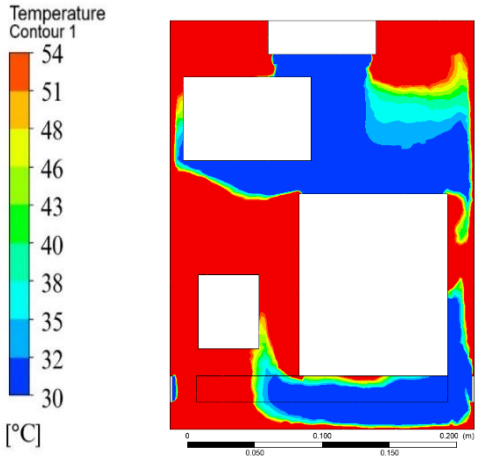	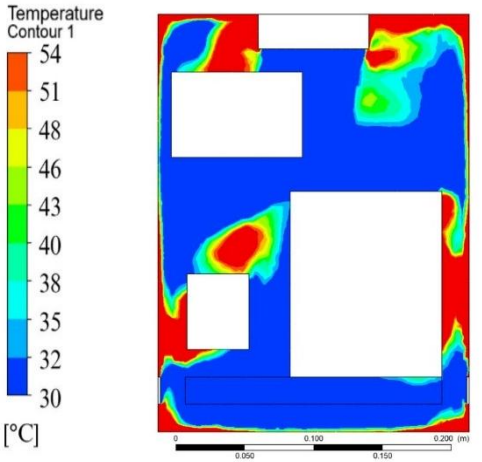	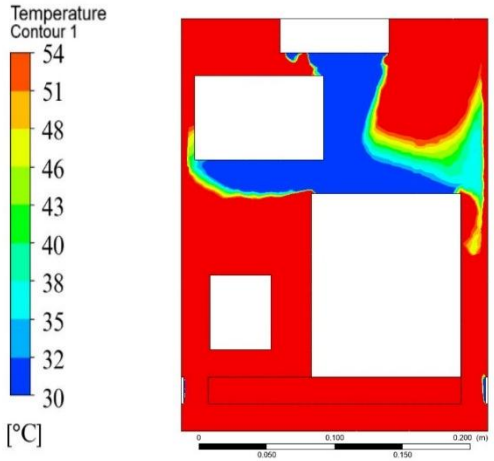
	Hotspots approximately 54 °C was observed around the temperature and humidity sensor (lower-left corner of the casing)	Improvement in CFM gradually reduced the high temperature regions approximately 54 °C around the temperature and humidity sensor to 30 °C Compare to References Case, Case 1 demonstrated that approximately 80% of the high temperature regions around the temperature and humidity sensor were eliminated with high CFM of the exhaust fan	Reduction in CFM led to a gradual expansion of the high temperature regions approximately 54 °C within the casing, especially on lower part of the casing Compare to References Case, Case 2 exhibited a larger area approximately 80% of the casing shows high temperature with low CFM of the exhaust fan

<table>
<tr>
<td>Airflow velocity contour on plane Z = 20 mm</td>
<td> 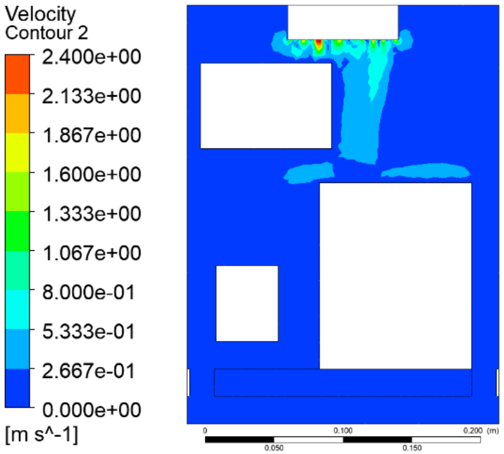

Air circulation was obstructed by the Raspberry Pi and PM sensor, resulting in lower airflow ranged from 0 m/s to 0.27 m/s around the temperature and humidity sensors, which led to stagnant air in this region</td>
<td> 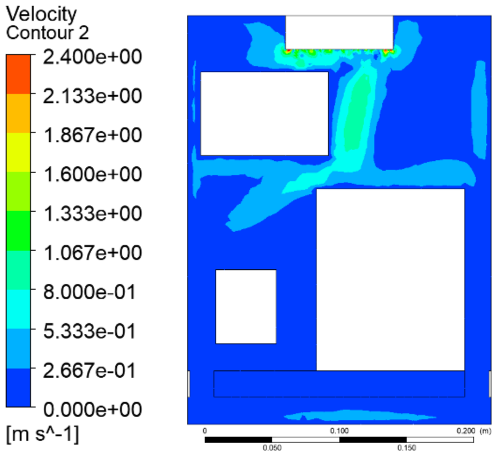

Improvement in CFM led to an increase in airflow velocity ranged from 0.27 m/s to 0.53 m/s and further enhanced air circulation around the temperature and humidity sensor

The enhancement in CFM, the maximum airflow velocity was improved from 0.27 m/s to 0.53 m/s</td>
<td> 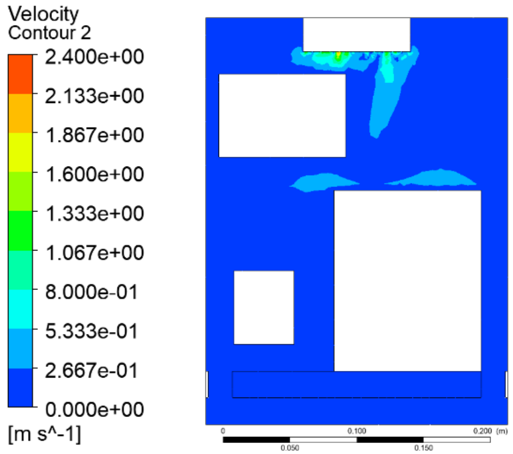

Reduction in CFM led to a lower airflow velocity ranged from 0 m/s to 0.27 m/s and resulted in the formation of larger stagnant air regions

The reduction in CFM resulted decrease in maximum airflow velocity from 0.8 m/s to 0.53 m/s.</td>
</tr>
</table>

5. Conclusions

This study successfully developed a real-time IoT-based OAQMS featuring a weather-resistant casing, specially designed to shield electronic components such as microcontrollers and sensors from adverse environmental conditions, including high humidity, solar radiation, and rain exposure. The casing integrates a DC exhaust fan to enhance internal ventilation and maintain safe operating temperatures, particularly under tropical climate conditions.

Through CFD simulations, the system thermal performance was optimized, revealing that a fan rated at 44.18 CFM provided the most effective cooling configuration. This setup maintained the internal casing temperature below 54 °C, effectively mitigating thermal buildup during peak solar exposure. Experimental validation for the sensors accuracy demonstrated high reliability, with percentage error of only 0.56% for temperature and 2.34% for relative humidity, confirming the system accuracy and stability under real operating conditions.

The finalised prototype offers a cost-effective, durable, and scalable solution for continuous outdoor air quality monitoring, particularly suited for tropical urban environments such as roadside stations, industrial zones, and public parks. For future development, further improvements are recommended, including refined airflow path design, integration of additional pollutant sensors (e.g., NO_2, CO_2, and O_3), and use of advanced materials such as UV-stabilized polymers or composite enclosures to enhance long-term durability. These advancements will extend the applicability of the system for smart city infrastructure, environmental research, and public health monitoring, contributing to global sustainability objectives aligned with UN SDGs 11 and 13.

Acknowledgment

The authors would like to acknowledge financial support from Asia Technological University (ATU) Network under ATU-Net Young Researcher Grant (YRG) with Vot. No. R.J130000.7724.4J714 and Universiti Teknologi Malaysia under UTM Nexus Postgrad with Vot no. Q.J130000.5324.00L96.

References

[1] Yang, X., et al., *NO2 Emissions at Highway Toll Stations: Integrated Satellite and Traffic Data Insights from Holiday Analysis.* Water, Air, & Soil Pollution, 2025. **236**(7): p. 458.
[2] *Ambient (outdoor) air pollution*. 2024 [cited 2025 3 March]; Available from: https://www.who.int/news-room/fact-sheets/detail/ambient-(outdoor)-air-quality-and-health#:~:text=Outdoor%20air%20pollution%20is%20a,key%20to%20protecting%20public%20health.
[3] Mangin, T., et al., *Understanding the effect of outdoor pollution episodes and HVAC type on indoor air quality.* Building and Environment, 2025. **278**: p. 112978.
[4] John, G., et al., *Air Pollution and Its Impact on Health and Performance in Football Players.* Sports, 2025. **13**(6): p. 170.
[5] Margiana, R., et al., *Does outdoor air pollution cause poor semen quality? A systematic review and meta-analysis.* BMC Urology, 2025. **25**(1): p. 50.
[6] Tan, H., et al., *Revolutionizing indoor air quality monitoring through IoT innovations: a comprehensive systematic review and bibliometric analysis.* Environmental Science and Pollution Research, 2024. **31**(32): p. 44463-44488.
[7] Wong, S.J., et al., *Optimizing indoor air quality: evaluating the synergistic impact of filter integration and botanical solutions.* Clean Technologies and Environmental Policy, 2025: p. 1-25.
[8] Spooner, M., et al., *A climate classification for corrosion control in electronic system design.* Machine Learning with Applications, 2022. **9**: p. 100397.
[9] Singh, D., et al., *Sensors and systems for air quality assessment monitoring and management: A review.* Journal of Environmental Management, 2021. **289**: p. 112510.
[10] Seesaard, T., K. Kamjornkittikoon, and C. Wongchoosuk, *A comprehensive review on advancements in sensors for air pollution applications.* Science of The Total Environment, 2024. **951**: p. 175696.
[11] Jabbar, W.A., et al., *LoRaWAN-Based IoT System Implementation for Long-Range Outdoor Air Quality Monitoring.* Internet of Things, 2022. **19**: p. 100540.
[12] Vélez-Guerrero, A.C., M. Callejas-Cuervo, and A.C. Alarcón-Aldana, *The Evolution of Air Quality Monitoring: Measurement Techniques and Instruments.* Journal of Hunan University Natural Sciences, 2023. **50**(5).
[13] Johnston, S.J., et al., *City Scale Particulate Matter Monitoring Using LoRaWAN Based Air Quality IoT Devices.* Sensors, 2019. **19**(1): p. 209.
[14] Collado, E., et al., *Open-source Internet of Things (IoT)-based air pollution monitoring system with protective case for tropical environments.* HardwareX, 2024. **19**: p. e00560.

[15] Yi, W.Y., et al., *A Survey of Wireless Sensor Network Based Air Pollution Monitoring Systems.* Sensors, 2015. **15**(12): p. 31392-31427.
[16] Correia, C., et al., *Advancing air quality monitoring: A low-cost sensor network in motion – Part I.* Journal of Environmental Management, 2024. **360**: p. 121179.
[17] He, Z., D. Kwon, and M. Pecht, *Evaluation of IEC 60529 as a standard for liquid protection assessment of portable electronics.* e-Prime - Advances in Electrical Engineering, Electronics and Energy, 2025. **12**: p. 100952.
[18] *PM sensors*. Available from: https://www.renkeer.com/product/pm-sensor/
[19] *Temperature sensors*. Available from: https://www.renkeer.com/product/modbus-rtu-temperature-sensor/
[20] *Raspberry pi*. Available from: https://www.raspberrypi.com/products/raspberry-pi-4-model-b/.
[21] *DC 5V exhaust fan*
[22] Peng, Y., et al., *Experimental investigation for performance of high-strength bolt shear connections with fasteners embedded in aluminum alloy plates.* Structures, 2025. **71**: p. 108081.
[23] Lai, B., et al., *Accuracy and Precision of Three Consumer-Grade Motion Sensors During Overground and Treadmill Walking in People With Parkinson Disease: Cross-Sectional Comparative Study.* JMIR Rehabil Assist Technol, 2020. **7**(1): p. e14059.
[24] Ismail, N.D., et al., *Energy-efficient ventilation strategies at hospital front desks for minimizing infectious particle dispersion: Considering patient postures and airflow optimization.* Energy, 2024. **307**: p. 132822.
[25] Wittek, A. and K. Miller, *Chapter 39 - Computational biomechanics for medical image analysis*, in *Handbook of Medical Image Computing and Computer Assisted Intervention*, S.K. Zhou, D. Rueckert, and G. Fichtinger, Editors. 2020, Academic Press. p. 953-977.
[26] Tan, H., et al., *Utilising localised exhaust and air curtain to reduce airborne particle settlement on surgical patients: potential future application in operating rooms?* Journal of Thermal Analysis and Calorimetry, 2024.
[27] Wong, K.Y., et al., *Effects of medical staff's turning movement on dispersion of airborne particles under large air supply diffuser during operative surgeries.* Environmental Science and Pollution Research, 2022.
[28] Boukhanouf, R. and A. Haddad, *A CFD analysis of an electronics cooling enclosure for application in telecommunication systems.* Applied Thermal Engineering, 2010. **30**(16): p. 2426-2434.
[29] Tan, H., et al., *Does human movement-induced airflow elevate infection risk in burn patient's isolation ward? A validated dynamics numerical simulation approach.* Energy and Buildings, 2023. **283**: p. 112810.
[30] Zhao, B., et al., *How Many Airborne Particles Emitted from a Nurse will Reach the Breathing Zone/Body Surface of the Patient in ISO Class5 Single-Bed Hospital Protective Environments?—A Numerical Analysis.* Aerosol Science and Technology - AEROSOL SCI TECH, 2009. **43**: p. 990-1005.